Integrity of neurocognitive networks in dementing disorders as measured with simultaneous PET/fMRI

Isabelle Ripp[1]*, Thomas Stadhouders[1]*, Alexandre Savio[1], Oliver Goldhardt[2], Jorge Cabello[1], Vince Calhoun[3,4], Valentin Riedl[5,6], Dennis Hedderich[5], Janine Diehl-Schmid[2], Timo Grimmer[2], Igor Yakushev[1,6]

* *equally contributed*

[1] Department of Nuclear Medicine, Klinikum rechts der Isar, Technical University of Munich, Germany

[2] Department of Psychiatry and Psychotherapy, Klinikum rechts der Isar, Technical University of Munich, Germany

[3] Department of Electrical and Computer Engineering, University of New Mexico, Albuquerque, New Mexico, USA

[4] The Mind Research Network and LBERI, Albuquerque, New Mexico, USA

[5] Department of Neuroradiology, Klinikum rechts der Isar, Technical University of Munich, Germany

[6] Neuroimaging Center (TUM-NIC), Klinikum rechts der Isar, Technical University of Munich, Germany

Running title: Neurocognitive Networks in Dementia

Corresponding author:
Igor Yakushev, MD
Dept. of Nuclear Medicine
Technical University of Munich
Ismaninger Str. 22
81675 Munich
Phone: +49 (0) 89-4140-6085
Fax: +49 (0) 89-4140-7431
Email: igor.yakushev@tum.de

First author:

Isabelle Ripp

Dept. of Nuclear Medicine

Technical University of Munich

Ismaninger Str. 22

81675 Munich

Phone: +49 (0) 89-4140-7971

Email: isabelle.ripp@tum.de

ABSTRACT

Background: Functional magnetic resonance imaging (fMRI) studies have reported altered integrity of large-scale neurocognitive networks (NCNs) in dementing disorders. However, findings on specificity of these alterations in patients with Alzheimer's disease (AD) and behavioral variant frontotemporal dementia (bvFTD) are still very limited. Recently, NCNs have been successfully captured using positron emission tomography (PET) with F18-fluordesoxyglucose (FDG). **Methods:** Network integrity was measured in 72 individuals (38 male) with mild AD, bvFTD, and healthy controls using a simultaneous resting state fMRI and FDG-PET. Indices of network integrity were calculated for each subject, network, and imaging modality. **Results**: In either modality, independent component analysis revealed four major NCNs: anterior default mode network (DMN), posterior DMN, salience network, and right central executive network (CEN). In fMRI data, integrity of posterior DMN was found to be significantly reduced in both patient groups relative to controls. In the AD group anterior DMN and CEN appeared to be additionally affected. In PET data, only integrity of posterior DMN in patients with AD was reduced, while three remaining networks appeared to be affected only in patients with bvFTD. In a logistic regression analysis, integrity of anterior DMN as measured with PET alone accurately differentiated between the patient groups. A correlation between indices of two imaging modalities was overall low. **Conclusions:** FMRI and FDG-PET capture partly different aspects of network integrity. A higher disease specificity of NCNs as derived from PET data supports metabolic connectivity imaging as a promising diagnostic tool.

Key words: Alzheimer's disease, frontotemporal dementia, positron emission tomography, multimodal neuroimaging, resting state networks

INTRODUCTION

In the last decades, resting state networks (RSNs) have been a hot topic of cognitive and clinical neuroscience. Using resting state functional magnetic resonance imaging (fMRI), abnormalities in so called neurocognitive networks (NCNs) have been found in numerous neuropsychiatric disorders (*1*). Neurodegenerative diseases including dementia are not an exception (*2,3*). In their seminal paper, Greicius et al. (*4*) reported decreased functional connectivity (FC) of the default mode network (DMN) in patients with Alzheimer's disease (AD) as compared to healthy subjects. A further study suggested even a differential disruption of network connectivity in dementing disorders. Thus, DMN was reported to be affected in AD, while salience network (SN) in behavioral variant frontotemporal disease (bvFTD) (*5*). However, observations on this topic have been rather inconsistent. For instance, reduced in-phase connectivity with DMN was found in patients with bvFTD (*6*). Others reported an increased FC within the frontal networks in AD subjects (*7*). In agreement with these heterogeneous results the clinical applicability of resting state fMRI remains very limited. Among putative reasons are a low signal-to-noise ratio and reproducibility of the findings at a single subject level (*8*). Positron emission tomography (PET) with 18F-fluorodeoxyglucose (FDG) is an established clinical tool for early and differential diagnosis of dementing and movement disorders (*9,10*). While multivariate decomposition of PET data has been successfully applied in both neurodegenerative dementia (*11*) and Parkinsonian syndromes (*12*) RSNs could be identified in FDG-PET data only recently (*13–16*). In particular, our group has found spatially similar RSNs in fMRI and FDG-PET data in the same group of healthy subjects (*15*). The present study addressed the value of FDG-PET in assessing integrity of NCNs in dementing disorders, in comparison with fMRI. To this end, resting state fMRI and FDG-PET data were acquired simultaneously in the same group of patients with AD, bvFTD and healthy controls (HC). Of note, a simultaneous data acquisition allows to minimize variability in RSNs due to different brain states, excitement level or mood of the person (*17,18*).

4

MATERIALS AND METHODS

Subjects

We retrospectively analyzed data of patients who were referred to our center for a PET/MR examination as part of a diagnostic work-up for suspected neurodegenerative disorder. Only subjects with an expert diagnosis of AD or bvFTD were considered. The expert diagnosis was made by a consensus of at least two experienced psychiatrists under consideration of a clinical examination, results of neuropsychological and lab testing, imaging and CSF biomarkers. The imaging biomarkers included structural MRI, FDG-PET, and in some cases amyloid PET. The diagnosis of AD was made according to the NINCDS-ADRDA (*19*) or NIA-AA (*20*) criteria. In the latter case, the clinical diagnosis of MCI due to AD was supported by AD-typical biomarker findings. BvFTD was diagnosed according to the recent diagnostic criteria (*21*). Only patients with a mini mental state examination (MMSE) score ≥18 were included. The group of HC consisted of individuals without psychiatric and neurological symptoms and no complaints about cognitive impairment. They were recruited mainly via advertisements in local newspapers.

The study was carried out in accordance with the latest version of the Declaration of Helsinki after the consent procedures had been approved by the local ethics committee of the medical faculty at the Technische Universität München (TUM). Written informed consent was obtained from all subjects.

Image data acquisition

Imaging was performed on a 3T Siemens Biograph mMR scanner (Siemens Healthineers AG, Erlangen, Germany) under standard resting conditions. Structural T1-weighted (MPRAGE) images were acquired using a three-dimensional (3D) normal gradient recalled sequence (repeat time (TR) 2300.0 ms; echo time (TE) 2.98 ms; 9.0º flip angle) measuring 160 sagittal slices (field of view (FOV) 240x256mm^2; pixel spacing 1 mm, 256x240 scan matrix, slice thickness 1.0 mm). Resting state fMRI was performed with the following parameters: TR 2.000 ms; TE 30 ms; flip angle 90°; 35 slices (gap 0.6 mm), aligned

to anterior/posterior commissure (AC/PC) covering the whole brain; FOV 192 mm; matrix size 64x64; voxel size 3.0x3.0x3.0 mm^3. PET acquisition ran in parallel for 15 minutes starting 30 minutes post injection i.v. of on average 198 (range 154-237) MBq. The subjects had fasted for at least 6 hours before scanning. Raw FDG-PET data were reconstructed using a filtered back-projection and filtered with an isotropic Hamming filter (5 mm full-width at half-maximum (FWHM)). Attenuation correction was performed using a default Dixon MRI sequence.

Image preprocessing

The image data were preprocessed mainly using SPM12 (Wellcome Trust Center for Neuroimaging, London, UK). After segmentation, T1 images were spatially normalized into the Montreal Neurological Institute (MNI) space. Echo-planar-imaging images were slice-time corrected, realigned, coregistered to subjects specific T1 images in MNI space and band-pass filtered (0.01 and 0.08 Hz). The first three images (6 s) of each subject's fMRI data were discarded to allow for equilibration of the magnetic field. In addition, a component-based noise correction (aCompCor) (22,23) based on CSF signal was applied. The applied pre-processing pipeline is available as an open source software tool (https://github.com/neurita/pypes/tree/v0.2.1) (24). To minimize a negative methodological bias towards fMRI data, a particular attention was paid to potential motion artifacts (supplementary material). FDG-PET images were spatially normalized to the MNI space using a study-specific FDG-PET template and smoothed with an 8 mm FWHM Gaussian kernel, in analogy with fMRI data. No correction for partial volume effects was applied. First, a uniform method for fMRI and FDG-PET data does not exist; different methods may have biased the results in favor of one imaging modality (25). Second, our analyses focused on larger cortical structures (networks), and patients with only mild disease severity, in whom a relevant atrophy is unlikely, were included.

Independent component analysis

To extract RSNs, a spatial independent component analysis (ICA) was applied independently to fMRI and PET data. Individual subject fMRI time-series images were concatenated for the group ICA (*26*). A concatenation of one mean PET image per subject was used for the group ICA (*13–15,27*). We applied a 30 components' ICA model for both imaging modalities. This intermediate model order (n=30) was chosen to extract robust spatial maps, preventing coherent RSNs to be splitted into several sub-networks (*28–30*). Based on the known perturbations in NCNs in dementing disorders (see introduction), we *a priori* focused analyses on the following networks of interest: DMN, SN, and central executive network (CEN). Following previous studies, the primary visual and auditory networks were chosen as reference networks, as they are supposed to be unaffected in AD and bvFTD, at least at a clinically mild disease stage (*31,32*). In both imaging modalities, relevant spatial maps were selected using a spatial correlation with established functional templates (*30*).

Indices of network integrity

In both imaging modalities, subject-specific spatial maps and time courses were estimated with a GICA3 back-reconstruction method, consisting of a two-step multiple regression (*33*). This method is based on a principle component analysis compression and projection (*26,34*). To derive individual indices of network integrity for fMRI data, a spatio-temporal regression – also called dual regression – was computed against group-based maps (*35,36*). For PET data, we computed so called loading coefficients, a degree of component (RSN) expression in individual subjects (*26,27*). Of note, a conceptually equivalent representation underlies network integrity measures of both imaging modalities. Details are provided in supplementary material. Finally, indices of network integrity were available for each subject, network, and imaging modality.

White matter hyperintensities and hemorrhages

Results of network analyses (see below) prompted us additional post-hoc analyses. First, we quantified a volume of white matter hyperintensities (WMH) upon T2 FLAIR images (*37*). Second, we assessed presence of eventual hemorrhages as index of (sporadic) cerebral amyloid angiopathy (CAA). To this end, an experienced neuroradiologist (DH) read T2*-weighted images for CAA according to established criteria (*38*).

Statistics

Integrity indices were compared between the groups independently for each modality using ANOVA with a post hoc 2-sample t-test. A $p<0.05$ Bonferroni corrected for multiple tests, i.e. RSNs of interest, was accepted as significance level. For explorative reasons we also present results with $p<0.05$ uncorrected. A binary logistic regression (step-wise) with resubstitution and cross-validation (leave-one-out classification) was performed to predict the diagnostic status (AD vs. bvFTD) using indices of network integrity (IBM SPSS statistics 22). An association between integrity indices of two modalities for the same network was tested using a non-parametric Spearman correlation. A non-parametric Mann-Whitney U test was applied to test for differences in WMH volume between the groups. A chi-quadrat-test was applied to test for differences in a proportion of subjects with CAA (possible and probable were pooled) between three groups. Results were considered significant at $p<0.05$.

RESULTS

Subjects

Following the inclusion criteria 72 subjects were selected for the study. Their demographic characteristics are summarized in Table 1. There was no significant difference for age, gender or MMSE between the groups. Thus, no correction for these variables was applied (*39*). The AD group included patients with MCI due to AD (n=19) and dementia due to AD (n=10).

Independent component analysis

Figure 1 depicts the RSNs of interest for each imaging modality. In both modalities, the DMN was split into the anterior and posterior networks. Only right CEN could be identified in PET data. Thus, further analyses focused on the following 6 networks: posterior DMN (pDMN), anterior DMN (aDMN), SN, right CEN, primary visual, and auditory.

------------------------------------- Figure 1 around here -------------------------------------

Resting state networks of interest

Figure 2 shows a distribution of the network integrity among the groups for each imaging modality. Note, each RSN (figure 1) was common for all subjects under the study, while network integrity measures were available in every single subject. In the FDG-PET data we observed a significantly lower integrity of aDMN and SN in bvFTD compared to AD. The integrity of pDMN was significantly higher in bvFTD compared to AD. In comparison to HC, the integrity of pDMN was significantly lower in AD, and the integrity of aDMN, SN and right CEN were significantly lower in bvFTD. For fMRI derived RSNs we observed a significantly lower integrity of pDMN, aDMN and right CEN in AD relative to HC. In bvFTD, a significantly lower integrity of pDMN compared to HC was found. At a $p<0.05$ uncorrected, integrity of each RSN of interest was lower in AD then in HC.

------------------------------------- Figure 2 around here -------------------------------------

Regression and correlation analyses

In fMRI data, integrity indices of the pDMN appeared as a single significant predictor of the diagnostic status, providing an accuracy of 64% (p=0.017; sensitivity 79%, specificity 43%). In PET data, aDMN was the strongest predictor with an accuracy of 94% (p=0.002; sensitivity 97%, specificity 91%), while addition of SN slightly but significantly increased the accuracy up to 96% (p=0.016;

sensitivity 97%, specificity 95%). The correlation analyses revealed at best a low within-network-between-modality correlation, with the highest R of 0.33 (p=0.005) for aDMN.

White matter hyperintensities and hemorrhages

The volume of WMH was 4.8±9.3, 2.6±2.9 and 2.7±3.9 ml in the AD, bvFTD and control group, respectively. There was no statistically significant difference between the groups (p>0.05). T2*-weighted images were available in 25 subjects with AD, all subjects with bvFTD, and 21 HC. In the AD group there were four subjects with possible and one subject with probable CAA. None of subjects with bvFTD appeared to have CAA. In the HC group possible CAA was diagnosed in one subject. The proportion of subjects with CAA was significantly larger in the AD group relative to the bvFTD (p=0.03), but not the HC group (p=0.13). There was no difference between the bvFTD and HC groups (p=0.31).

DISCUSSION

In the present study we examined integrity of NCNs in AD and bvFTD using simultaneous resting state fMRI and FDG-PET. Like in our previous work on healthy subjects (*15*), spatially similar RSNs were found in both imaging modalities. In PET data, integrity of NCNs was differentially affected in two dementing disorders. In fMRI data, all networks of interest showed the lowest integrity in AD, and a lower integrity in bvFTD relative to HC. Integrity of aDMN - as measured with FDG-PET - accurately discriminated between the two patient groups. Such a distinction was not possible using the same NCNs from fMRI data.

Whereas FDG-PET is supposed to capture neural/synaptic activity by estimating glucose consumption in terms of neurometabolic coupling (*40*), fMRI measures neural activity less directly, through amount of oxygen in blood supplying a given brain region (*41*). This so called neurovascular coupling is based on a complex interplay between local cerebral blood flow, volume, and cerebral metabolic rate of oxygen (*42*). Thus, the partly different findings in our fMRI and FDG-PET data, as

well as a low correlation between integrity measurements of fMRI- and PET-based networks, are not surprising. In particular, we observed a lower integrity across all fMRI-based NCNs plus primary visual network in both patients' groups relative to controls, with the AD group being consistently more impaired than the bvFTD group. The former observation may have both a biological and methodological background. Different neurodegenerative disorders are known to share common pathophysiological phenomena such as production of toxic oligomers that cause intercellular miscommunication (43,44). The toxic effects lead to a dissynchrony of network activity that may manifest as impaired RSN integrity (45). As compared to blood oxygenation level dependent (BOLD) fMRI, FDG-PET possesses a much lower temporal resolution. A snapshot of FDG delivery over minutes may be more robust to non-specific whole brain (e.g., toxic) effects. In addition, ICA on PET data as in the present study identifies brain regions sharing similar FDG uptake, rather than synchronicity of the BOLD signal fluctuations. Hence, relative to fMRI data, alterations in RSNs in FDG-PET data seem to be driven more by a disease-specific neurodegeneration. In the same vain and other than in fMRI data, integrity of reference (non-NCNs) RSNs in PET data appeared to be preserved.

As a further finding, integrity of RSNs in fMRI data was consistently more impaired in the AD group than in the bvFTD one. This can be explained for instance by a more profound cerebrovascular disease in AD, as well by (sporadic) CAA that is often associated with AD (46). Thus, neurovascular decoupling as measured with fMRI was shown to be associated with severity of CAA. Hereby patients with CAA had lower amplitude of the fMRI response within the visual cortex during a visual task compared with controls (47). That study also reported a correlation between the impaired fMRI amplitude and a higher WMH volume in CAA patients. Of note, a recent study reported a limited reproducibility of functional connectivity networks particularly in patients with cerebral small vessel disease (48). On one hand, due to vascular lesions routine pathways of functional connectivity may be at least in part replaced by other, less consistent routes (48). On the other hand, vascular pathology may affect the BOLD hemodynamic response, reducing interregional correlations (49,50). Further, altered DMN connectivity was shown to

be significantly correlated with WMH burden (*51*), next to other studies confirming the central role of the white matter lesions in disrupting functional connectivity (*52–54*). Our post-hoc analyses support this hypothesis. Specifically, patients with AD showed a nearly double amount of WMH than patients with bvFTD and HC. Yet, apparently due to a high variability in the AD group the difference was statistically not significant. Furthermore, the proportion of subjects with CAA was higher among patients with AD than in two other groups.

Overall, the pattern of NCN alterations in FDG-PET rather than in fMRI data is in agreement with the known pathological changes in AD and bvFTD. Thus, a posterior NCN such as pDMN appeared to be affected in AD, while anterior NCNs such as aDMN and SN were disturbed in bvFTD. The (right) CEN, covering both the anterior and posterior parts of the brain, was affected in bvFTD, in line with the known executive dysfunction in these patients (*55*). Of note, pDMN was consistently affected in both modalities, i.e., its integrity was significantly lower in AD than in bvFTD and HC. This observation agrees well with the fMRI literature (*4,56*). However, a significant difference in a test measure does not necessarily mean that this measure is accurate in respect to class prediction, or, in clinical terms, in respect to differential diagnosis. To address this issue, we performed a step-wise logistic regression analysis. Among fMRI-based NCNs, integrity of the pDMN appeared to be the only significant predictor of the diagnosis (AD vs. bvFTD) with an accuracy of only 64%. This result is well below the accuracy values of 100% reported by *Zhou et al.* (2010). Apart from methodological differences the discrepancy can be explained by smaller patients' groups (n=12 each) and by a more advanced disease in patients with AD (average MMSE score of 21.2 vs. 24.3 in our study) in Zhou et al. (*5*). As for NCNs extracted from PET data, integrity of aDMN appeared to be the strongest predictor of the diagnostic status, providing an accuracy of 94%. All other NCNs on their own were significant predictors, too, but with a lower accuracy (data not shown). In a step-wise logistic regression with all PET-based NCNs, integrity of SN slightly improved the discrimination (96% accuracy).

An advantage of our study are well characterized and matched groups of patients and HCs. Furthermore, the PET and fMRI data were acquired simultaneously, pre-processed and analyzed in an analogous manner. To minimize a negative bias towards fMRI, we applied a state of the art image analysis, with a special attention to the quality control of fMRI data (e.g., analyses of motion artifacts). As a limitation, our study focused on the established NCNs. However, other networks, e.g., limbic, may also be of relevance in neurodegenerative dementia in general, and in bvFTD in particular (*57*). Future studies should address this issue. As a further limitation, results of the logistic regression were cross-validated using a leave-one-out approach. Thus, they may be too optimistic; a prospective validation in another cohort is essential.

CONCLUSION

Our study provides novel insights into alterations of the established RSNs in AD and bvFTD, supporting metabolic connectivity imaging as a valuable tool in the field of brain connectivity. As a prospective, we propose to establish an atlas of FDG-PET-based RSNs similar to that by Allen et al. for fMRI (*30*). This would allow to characterize disease-specific connectivity patterns at the metabolic network level (*12,58–60*).

Acknowledgments

KEY POINTS:

QUESTION: What is the value of altered network integrity – as measured with FDG-PET and fMRI – in dementing disorders?

PERTINENT FINDINGS: The pattern of network alterations differed between the modalities, with the fMRI-based neurocognitive networks (NCNs) showing a generally lower disease specificity. Integrity of anterior default mode network as measured with PET alone accurately differentiated between patients with mild Alzheimer's disease and behavioral variant frontotemporal dementia.

IMPLICATIONS FOR PATIENT CARE: A higher disease specificity of NCNs as derived from PET data supports metabolic connectivity imaging as a promising diagnostic tool.

REFERENCES

1. Sha Z, Wager TD, Mechelli A, He Y. Common Dysfunction of Large-Scale Neurocognitive Networks Across Psychiatric Disorders. *Biological Psychiatry*. 2019;85:379-388.

2. Pievani M, Filippini N, van den Heuvel MP, Cappa SF, Frisoni GB. Brain connectivity in neurodegenerative diseases—from phenotype to proteinopathy. *Nature Reviews Neurology*. 2014;10:620-633.

3. Sala A, Perani D. Brain Molecular Connectivity in Neurodegenerative Diseases: Recent Advances and New Perspectives Using Positron Emission Tomography. *Front Neurosci*. 2019;13.

4. Greicius MD, Srivastava G, Reiss AL, Menon V. Default-mode network activity distinguishes Alzheimer's disease from healthy aging: evidence from functional MRI. *Proc Natl Acad Sci USA*. 2004;101:4637-4642.

5. Zhou J, Greicius MD, Gennatas ED, et al. Divergent network connectivity changes in behavioural variant frontotemporal dementia and Alzheimer's disease. *Brain*. 2010;133:1352-1367.

6. Whitwell JL, Josephs KA, Avula R, et al. Altered functional connectivity in asymptomatic MAPT subjects: a comparison to bvFTD. *Neurology*. 2011;77:866-874.

7. Agosta F, Pievani M, Geroldi C, Copetti M, Frisoni GB, Filippi M. Resting state fMRI in Alzheimer's disease: beyond the default mode network. *Neurobiol Aging*. 2012;33:1564-1578.

8. Lee MH, Smyser CD, Shimony JS. Resting-state fMRI: a review of methods and clinical applications. *AJNR Am J Neuroradiol*. 2013;34:1866-1872.

9. Bohnen NI, Djang DSW, Herholz K, Anzai Y, Minoshima S. Effectiveness and safety of 18F-FDG PET in the evaluation of dementia: a review of the recent literature. *J Nucl Med*. 2012;53:59-71.

10. Whitwell JL, Graff-Radford J, Singh TD, et al. 18F-FDG PET in Posterior Cortical Atrophy and Dementia with Lewy Bodies. *J Nucl Med*. 2017;58:632-638.

11. Nazem A, Tang CC, Spetsieris P, et al. A multivariate metabolic imaging marker for behavioral variant frontotemporal dementia. *Alzheimers Dement (Amst)*. 2018;10:583-594.

12. Schindlbeck KA, Eidelberg D. Network imaging biomarkers: insights and clinical applications in Parkinson's disease. *Lancet Neurol*. 2018;17:629-640.

13. Di X, Biswal BB, Alzheimer's Disease Neuroimaging Initiative. Metabolic brain covariant networks as revealed by FDG-PET with reference to resting-state fMRI networks. *Brain Connect*. 2012;2:275-283.

14. Yakushev I, Chételat G, Fischer FU, et al. Metabolic and structural connectivity within the default mode network relates to working memory performance in young healthy adults. *Neuroimage*. 2013;79:184-190.

15. Savio A, Fünger S, Tahmasian M, et al. Resting-State Networks as Simultaneously Measured with Functional MRI and PET. *J Nucl Med*. 2017;58:1314-1317.

16. Trotta N, Baete K, Van Laere K, Goldman S, De Tiège X, Wens V. Letter to the Editor: Neurometabolic resting-state networks derived from seed-based functional connectivity analysis. *J Nucl Med*. April 2018.

17. Waites AB, Stanislavsky A, Abbott DF, Jackson GD. Effect of prior cognitive state on resting state networks measured with functional connectivity. *Human Brain Mapping*. 2005;24:59-68.

18. Harrison BJ, Pujol J, Ortiz H, Fornito A, Pantelis C, Yücel M. Modulation of brain resting-state networks by sad mood induction. *PLoS ONE*. 2008;3:e1794.

19. McKhann G, Drachman D, Folstein M, Katzman R, Price D, Stadlan EM. Clinical diagnosis of Alzheimer's disease: report of the NINCDS-ADRDA Work Group under the auspices of Department of Health and Human Services Task Force on Alzheimer's Disease. *Neurology*. 1984;34:939-944.

20. Albert MS, DeKosky ST, Dickson D, et al. The diagnosis of mild cognitive impairment due to Alzheimer's disease: recommendations from the National Institute on Aging-Alzheimer's Association workgroups on diagnostic guidelines for Alzheimer's disease. *Alzheimers Dement*. 2011;7:270-279.

21. Rascovsky K, Hodges JR, Knopman D, et al. Sensitivity of revised diagnostic criteria for the behavioural variant of frontotemporal dementia. *Brain*. 2011;134:2456-2477.

22. Behzadi Y, Restom K, Liau J, Liu TT. A component based noise correction method (CompCor) for BOLD and perfusion based fMRI. *Neuroimage*. 2007;37:90-101.

23. Muschelli J, Nebel MB, Caffo BS, Barber AD, Pekar JJ, Mostofsky SH. Reduction of motion-related artifacts in resting state fMRI using aCompCor. *Neuroimage*. 2014;96:22-35.

24. Savio AM, Schutte M, Graña M, Yakushev I. Pypes: Workflows for Processing Multimodal Neuroimaging Data. *Front Neuroinform*. 2017;11.

25. van Golen LW, Kuijer JPA, Huisman MC, et al. Quantification of cerebral blood flow in healthy volunteers and type 1 diabetic patients: comparison of MRI arterial spin labeling and [(15)O]H2O positron emission tomography (PET). *J Magn Reson Imaging*. 2014;40:1300-1309.

26. Calhoun VD, Adali T, Pearlson GD, Pekar JJ. A method for making group inferences from functional MRI data using independent component analysis. *Hum Brain Mapp*. 2001;14:140-151.

27. Shaffer JL, Petrella JR, Sheldon FC, et al. Predicting Cognitive Decline in Subjects at Risk for Alzheimer Disease by Using Combined Cerebrospinal Fluid, MR Imaging, and PET Biomarkers. *Radiology*. 2013;266:583-591.

28. Jafri MJ, Pearlson GD, Stevens M, Calhoun VD. A method for functional network connectivity among spatially independent resting-state components in schizophrenia. *Neuroimage*. 2008;39:1666-1681.

29. Biswal BB, Mennes M, Zuo X-N, et al. Toward discovery science of human brain function. *Proc Natl Acad Sci USA*. 2010;107:4734-4739.

30. Allen EA, Erhardt EB, Damaraju E, et al. A baseline for the multivariate comparison of resting-state networks. *Front Syst Neurosci*. 2011;5:2.

31. Zamboni G, Wilcock GK, Douaud G, et al. Resting Functional Connectivity Reveals Residual Functional Activity in Alzheimer's Disease. *Biological Psychiatry*. 2013;74:375-383.

32. Santens P, De Bleecker J, Goethals P, et al. Differential regional cerebral uptake of (18)F-fluoro-2-deoxy-D-glucose in Alzheimer's disease and frontotemporal dementia at initial diagnosis. *Eur Neurol*. 2001;45:19-27.

33. Erhardt EB, Rachakonda S, Bedrick E, Allen E, Adali T, Calhoun VD. Comparison of multi-subject ICA methods for analysis of fMRI data. *Hum Brain Mapp*. 2011;32:2075-2095.

34. Calhoun VD, Pekar JJ, McGinty VB, Adali T, Watson TD, Pearlson GD. Different activation dynamics in multiple neural systems during simulated driving. *Hum Brain Mapp*. 2002;16:158-167.

35. Beckmann CF, Mackay CE, Filippini N, Smith SM. Group comparison of resting-state FMRI data using multi-subject ICA and dual regression. *NeuroImage*. 2009;Supplement 1:S148.

36. Calhoun VD, Adalı T. Multisubject independent component analysis of fMRI: a decade of intrinsic networks, default mode, and neurodiagnostic discovery. *IEEE Rev Biomed Eng*. 2012;5:60-73.

37. Schmidt P, Gaser C, Arsic M, et al. An automated tool for detection of FLAIR-hyperintense white-matter lesions in Multiple Sclerosis. *Neuroimage*. 2012;59:3774-3783.

38. Linn J, Halpin A, Demaerel P, et al. Prevalence of superficial siderosis in patients with cerebral amyloid angiopathy. *Neurology*. 2010;74:1346-1350.

39. Spector PE, Brannick MT. Methodological Urban Legends: The Misuse of Statistical Control Variables. *Organizational Research Methods*. 2011;14:287-305.

40. Magistretti PJ, Allaman I. A cellular perspective on brain energy metabolism and functional imaging. *Neuron*. 2015;86:883-901.

41. Chen JJ. Functional MRI of brain physiology in aging and neurodegenerative diseases. *NeuroImage*. May 2018.

42. Kim S-G, Ogawa S. Biophysical and physiological origins of blood oxygenation level-dependent fMRI signals. *J Cereb Blood Flow Metab*. 2012;32:1188-1206.

43. Eisen A, Turner MR. Does variation in neurodegenerative disease susceptibility and phenotype reflect cerebral differences at the network level? *Amyotroph Lateral Scler Frontotemporal Degener*. 2013;14:487-493.

44. Warren JD, Rohrer JD, Schott JM, Fox NC, Hardy J, Rossor MN. Molecular nexopathies: a new paradigm of neurodegenerative disease. *Trends Neurosci*. 2013;36:561-569.

45. Ahmed RM, Devenney EM, Irish M, et al. Neuronal network disintegration: common pathways linking neurodegenerative diseases. *J Neurol Neurosurg Psychiatry*. 2016;87:1234-1241.

46. Jellinger KA. Alzheimer disease and cerebrovascular pathology: an update. *J Neural Transm (Vienna)*. 2002;109:813-836.

47. Peca S, McCreary CR, Donaldson E, et al. Neurovascular decoupling is associated with severity of cerebral amyloid angiopathy. *Neurology*. 2013;81:1659-1665.

48. Lawrence AJ, Tozer DJ, Stamatakis EA, Markus HS. A comparison of functional and tractography based networks in cerebral small vessel disease. *Neuroimage Clin*. 2018;18:425-432.

49. Mark CI, Mazerolle EL, Chen JJ. Metabolic and vascular origins of the BOLD effect: Implications for imaging pathology and resting-state brain function. *J Magn Reson Imaging*. 2015;42:231-246.

50. Williams RJ, Goodyear BG, Peca S, et al. Identification of neurovascular changes associated with cerebral amyloid angiopathy from subject-specific hemodynamic response functions. *J Cereb Blood Flow Metab*. 2017;37:3433-3445.

51. Wu M, Andreescu C, Butters MA, Tamburo R, Reynolds CF, Aizenstein H. Default-mode network connectivity and white matter burden in late-life depression. *Psychiatry Res*. 2011;194:39-46.

52. Aizenstein HJ, Andreescu C, Edelman KL, et al. fMRI correlates of white matter hyperintensities in late-life depression. *Am J Psychiatry*. 2011;168:1075-1082.

53. Steffens DC, Taylor WD, Denny KL, Bergman SR, Wang L. Structural integrity of the uncinate fasciculus and resting state functional connectivity of the ventral prefrontal cortex in late life depression. *PLoS ONE*. 2011;6:e22697.

54. Andreescu C, Tudorascu DL, Butters MA, et al. Resting state functional connectivity and treatment response in late-life depression. *Psychiatry Res*. 2013;214.

55. Elderkin-Thompson V, Boone KB, Hwang S, Kumar A. Neurocognitive profiles in elderly patients with frontotemporal degeneration or major depressive disorder. *J Int Neuropsychol Soc*. 2004;10:753-771.

56. Binnewijzend MAA, Schoonheim MM, Sanz-Arigita E, et al. Resting-state fMRI changes in Alzheimer's disease and mild cognitive impairment. *Neurobiol Aging*. 2012;33:2018-2028.

57. Malpetti M, Carli G, Sala A, et al. Variant-specific vulnerability in metabolic connectivity and resting-state networks in behavioural variant of frontotemporal dementia. *Cortex*. 2019;120:483-497.

58. Pagani M, Giuliani A, Öberg J, et al. Progressive Disintegration of Brain Networking from Normal Aging to Alzheimer Disease: Analysis of Independent Components of 18F-FDG PET Data. *J Nucl Med*. 2017;58:1132-1139.

59. Tomasi DG, Shokri-Kojori E, Wiers CE, et al. Dynamic brain glucose metabolism identifies anti-correlated cortical-cerebellar networks at rest. *J Cereb Blood Flow Metab*. January 2017:271678X17708692.

60. Yakushev I, Drzezga A, Habeck C. Metabolic connectivity: methods and applications. *Curr Opin Neurol*. 2017;30:677-685.

Figure 1: Resting state networks of interest
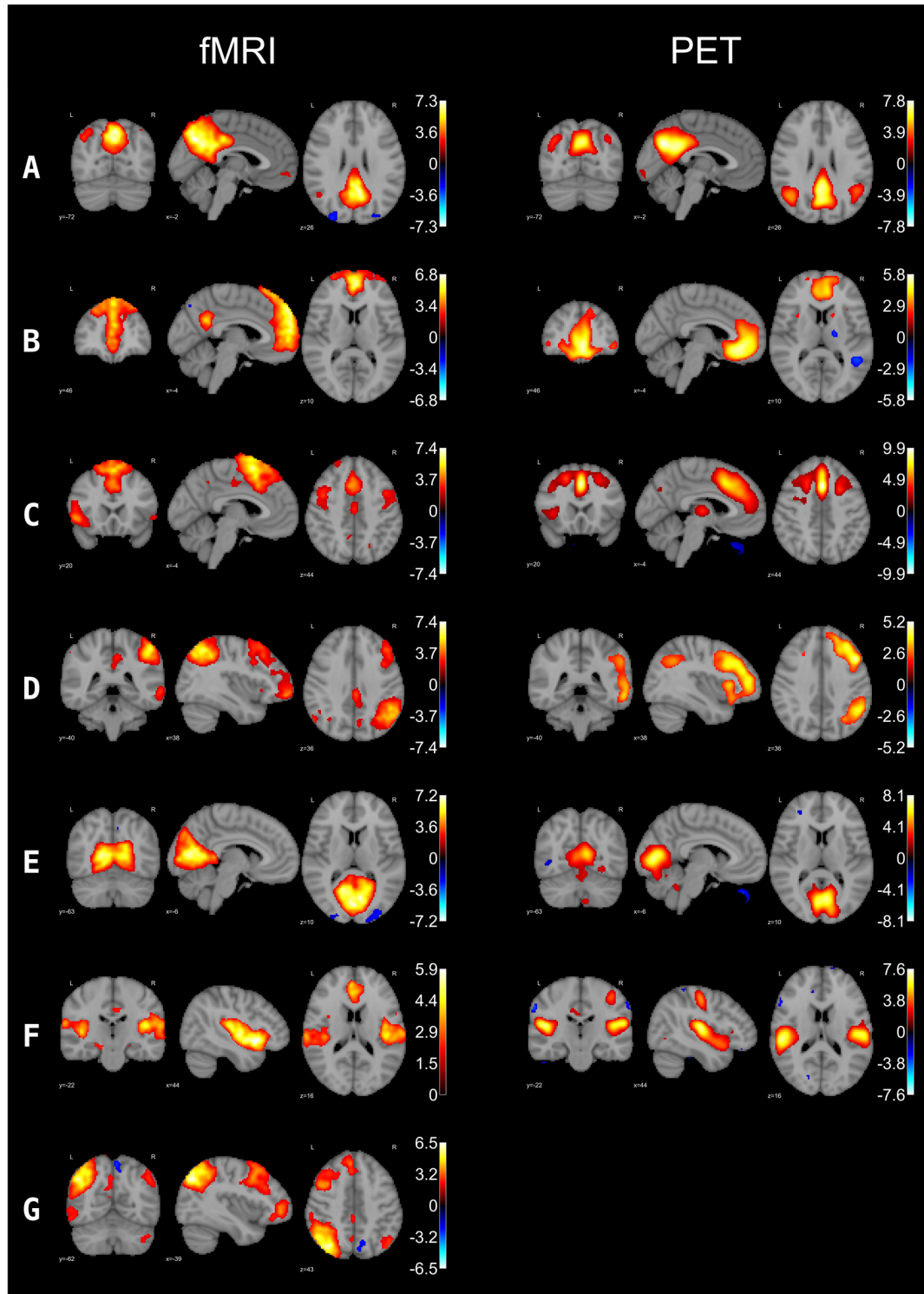
Overlay of IC maps at a threshold of *z*>2.0 on a T1 template in the MNI space. The color bar represents z-values. A) posterior default mode network, B) anterior default mode network, C) salience network, D) right central executive network, E) primary visual, F) auditory, G) left central executive network

Figure 2: Distribution of network integrity indices
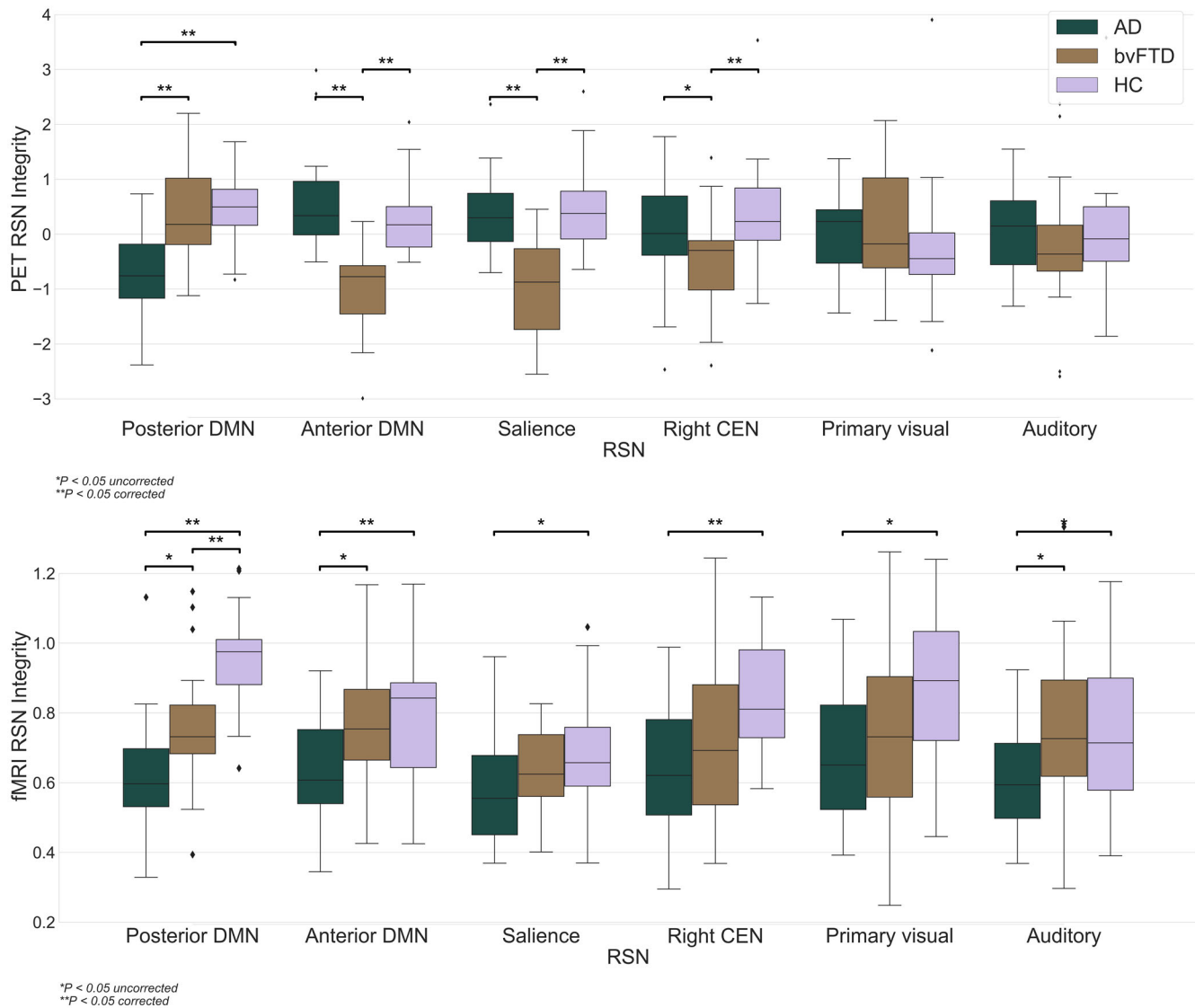
The boxes show the quartiles of the dataset while the whiskers extend to show the rest of the distribution, except for points that are determined to be "outliers" using a method that is a function of the inter-quartile range. Y-axis indicates a spatio-temporal regression for fMRI and loading coefficients for FDG-PET, respectively. Both indicate an individual degree of network integrity.

Table 1: Demographics

	AD	bvFTD	HC	p-value
N	29	21	22	-
M/F	11/18	15/6	12/10	0.055*
Age	64.3 ± 5.8	61.8 ± 9.4	60.4 ± 9.2	0.227**
MMSE	24.3 ± 3.0	25.5 ± 3.3	n.a.	0.660***

AD, Alzheimer's disease; bvFTD, behavioral variant frontotemporal dementia; HC, healthy control subjects; MMSE, mini mental state examination; n.a., not available. *Chi-quadrat test, **one-way ANOVA, ***t-test.

Supplemental material

Analyzes of motion artifacts

A Rapidart ArtifactDetect algorithm from NiPype (*1*) was used for signal nuisance correction by regressing out motion and intensity artifacts, if present (*2*). The tool computes the movement of the center of each face of a cuboid centered around the head and returns the maximal movement across the center. It is also implemented in Artifact Detection Tools (http://web.mit.edu/swg/software.htm). The following measures were recorded: total number of volumes that are affected by movement (motion outliers), maximum norm of the movement vector (maximum norm), and the standard deviation of the movement norms of the subjects. Four patients with AD, 5 patients with bvFTD, and no HC were discarded from further analyses due to a significant movement. This was defined as more than 30 motion outliers, a maximum norm larger than 4 mm, or a standard deviation larger than 1 mm.

Independent component analysis

We used the GIFT toolbox v3.0a (Medical Imaging Analysis Lab, The Mind Research Network; http://mialab.mrn.org/software/gift). Basically, ICA attempts to decompose the linearly mixed signals from the temporal dimension into independent spatial sources which are maximally independent non-Gaussian signals. As a first step of subject-specific data whitening and reduction a principal component analysis (PCA) is performed. After this, a group data reduction step retaining the number of PCs defined using the expectation-maximization algorithm to avoid prohibitive memory requirements (*3*). Aggregate spatial correlation maps are estimated as the centrotypes of component clusters to reduce sensitivity to initial algorithm parameters.

Calculation of loading coefficients

ICA is a data driven method which extracts a set of components from a set of a mixed signal observations. The independent components are orthogonal to each other. Therefore, the different n component signals s = [s1, s2, … sn] are assumed to be independent, but linearly mixed in m observations. The generative model x = As, where A is the mixing matrix, separates the different signals. Hereby, the elements of A represent the loading coefficients measuring a subject's spatial deviation from an average group derived component, i.e. RSN. Because the extracted components are expressed in individual subjects to a different degree, the mixing matrix entries (elements of A), i.e. the loading coefficients or integrity values, represent the spatial overlap between every subject's specific RSN and the equivalent group based RSN (4,5). Herewith, loading coefficients around zero represent a strong coherence between the subject specific and group-based RSN. For fMRI derived RSN the network integrity is quantified as the multiple (spatio-temporal) regression coefficient between a given group derived RSN and the equivalent subjects' specific RSN. Herewith, regression values around one represent a strong coherence between the subject specific and group based RSN.

REFERENCES

1.   Gorgolewski K, Burns CD, Madison C, et al. Nipype: a flexible, lightweight and extensible neuroimaging data processing framework in python. Front Neuroinformatics. 2011;5:13.

2.   NITRC: RapidArt: Tool/Resource Info. https://www.nitrc.org/projects/rapidart/.

3.   Rachakonda S, Silva RF, Liu J, Calhoun VD. Memory Efficient PCA Methods for Large Group ICA. Front Neurosci. 2016;10:17.

4.   Shaffer JL, Petrella JR, Sheldon FC, et al. Predicting Cognitive Decline in Subjects at Risk for Alzheimer Disease by Using Combined Cerebrospinal Fluid, MR Imaging, and PET Biomarkers. Radiology. 2013;266:583-591.

5.   Calhoun VD, Adali T, Pearlson GD, Pekar JJ. A method for making group inferences from functional MRI data using independent component analysis. Hum Brain Mapp. 2001;14:140-151.